Controlling structure and morphology of CoPt nanoparticles through dynamical or static coalescence effects

J. Penuelas, Pascal Andreazza, C. Andreazza-Vignolle, H.C.N. Tolentino, M. de Santis, C. Mottet

Controlling Structure and Morphology of CoPt Nanoparticles through Dynamical or Static Coalescence Effects

J. Penuelas,[1] P. Andreazza,[1,*] C. Andreazza-Vignolle,[1] H. C. N. Tolentino,[2] M. De Santis,[2] and C. Mottet[3]

[1]*Centre de Recherche sur la Matière Divisée, UMR 6619 Université d'Orléans & CNRS, 1 bis, rue de la Férollerie, 45071 Orléans Cedex, France*

[2]*Institut Néel, CNRS & UJF, 25 avenue des Martyrs BP 166, 38042 Grenoble Cedex 9, France*

[3]*Centre de Recherche en Matière Condensée et Nanosciences-CNRS, Campus de Luminy, case 913, 13288 Marseille Cedex 9, France*

(Received 12 November 2007; published 18 March 2008)

The structure and morphology of 1 to 3 nm size CoPt nanoparticles have been investigated *in situ* and in real time under different conditions: growth at 500 °C or at room temperature (RT) followed by annealing at 500 °C. The small-angle x-ray scattering measurements show size and temperature dependent growth mode with particle motions on the surface, while wide-angle scattering results, supported by Monte Carlo simulations, allow structure identification. If icosahedra are systematically detected at the first growth stages at RT, annealing at 500 °C yields the decahedral structure from the quasistatic coalescence of icosahedral morphology. Meanwhile, growth at 500 °C proceeds by a dynamical coalescence mechanism at the early stage, yielding truncated octahedral cubic structures.

DOI: 10.1103/PhysRevLett.100.115502 PACS numbers: 61.46.Df, 61.82.Bg, 64.70.Nd, 68.55.A−

Magnetic nanoparticles (NPs) have attracted a lot of interest because of their applications in ultrahigh density recording media. In particular, FePt and CoPt NPs are especially promising due to the combination of size reduction and alloying effects, which lead to an enhancement of both their magnetic moment and anisotropy [1,2]. Apart from size effects, their magnetic behavior is governed by chemical composition [2,3] and influenced by the degree of chemical order or segregation and by morphology [4–6]. These latter parameters are highly dependent on kinetic processes during the NPs formation. Indeed, metastable multitwinned structures, such as large icosahedra or decahedra [7], as well as metastable chemical arrangements, such as onionlike clusters [8], may occur. To achieve suitable magnetic performances, thermal annealing, during or after the NPs growth, is often required [1]. Such thermal assistance may induce morphological changes [9] or important chemical rearrangements in the NPs [10,11]. Moreover, in the case of supported NPs, it may also modify their size and dispersion on the substrate by coalescence or Ostwald ripening. Thus, it is of primary importance to understand temperature effects on the NPs formation mechanisms since their properties are directly connected to their structure and spatial organization.

In this Letter we focus on the morphology and structure of 1 to 3 nm supported CoPt NPs studied *in situ* and in real time by grazing incidence small-angle x-ray scattering (GISAXS) and grazing incidence x-ray diffraction (GIXD). The growth temperature effect, and the result of 500 °C annealing, is reported in terms of the mobility of atoms and particles and in terms of their structural evolution. For such temperature and cluster size ranges, morphological and structural changes occur without long range chemical ordering [6,11,12]. GISAXS and GIXD can make a statistical analysis of the morphology, structure and chemical order of NPs over the whole sample [13]. Grazing incidence ensures a minimum probing depth, so that surface mechanisms may be studied with high sensitivity. *In situ* analysis under ultrahigh vacuum (UHV) is also of prime importance because of the high reactivity of CoPt NPs with their environment that affects their morphology and structure [12]. Time scales for each growth step (nucleation, coarsening, or coalescence) are large enough to allow real time experiments and to study dynamical processes. We demonstrate that irrespective of the chemical ordering, the role of coalescence prevails over size-dependent morphology and structure and yields decahedral or face centered cubic (fcc) structures according to the thermal treatment.

The experiments were performed using the UHV setup of the French-CRG (BM32) beam line at the European Synchrotron Radiation Facility, which combines molecular beam epitaxy (MBE) growth with GISAXS and GIXD techniques [13]. The 18 keV monochromatic x-ray beam was set at a grazing incidence angle α_i of 0.07° with respect to the sample surface. Two-dimensional GISAXS patterns were recorded with a CCD camera mounted at 1 m behind the sample. For the GIXD measurements, a standard scintillator detector was set at a fixed exit angle related to the sample surface ($\alpha_e = \alpha_i$) and the scattering vector q was changed by scanning the in-plane angle. Co and Pt atoms were codeposited by MBE under a pressure varying from 2 to 5×10^{-10} mbar depending on the deposition or annealing temperature. The amorphous SiO_2 substrate was covered with a 10 nm-thick amorphous carbon (a-C) film. Such film limits cluster-to-substrate interactions and allows comparisons with our previous transmission electron microscopy (TEM) results [11]. Co and Pt deposition rates [0.26×10^{15} atoms/(cm^2 h) for each kind of atom] were adjusted to yield a composition close to $Co_{50}Pt_{50}$ with a constant flux of atoms during all the growth stages.

Real time GISAXS measurements were performed with an interval of 30 min between each recording. Beyond 1 h of deposition time on the substrate held at 500 °C, the 2D GISAXS pattern exhibits two distinct lobes of scattered intensity [Fig. 1(a)] that are proportional to the form factor $F(q)$ and the interference function $S(q)$ of cluster assembly. $F(q)$ represents the Fourier transform (FT) of the particle shape and $S(q)$, the FT of the cluster-cluster pair correlation function so that the size, shape, and correlation distance Λ of the NPs can be extracted by simulations using ISGISAXS software [14] from the $q_\perp$ and $q_\parallel$ cross sections [Fig. 1(b)]. The form factor is calculated in the distorted-wave Born approximation, which includes substrate reflections of the scattered intensity and allows fitting the Yoneda peak [15]. The NPs have a truncated spherical shape with an aspect ratio $H/D < 1$ at the beginning of the growth, where D and H are the NPs diameter and height, respectively. The size distribution has been fitted using a narrow Gaussian function with a geometrical standard deviation of $\sigma(D)/D = 0.3$ according to our previous TEM results [11]. The evolution of D and H with time for NPs grown at 500 °C was derived [Fig. 2(a)] from that of the cross sections [Figs. 1(c) and 1(d)]. D increases as a power law during the deposition, the exponent (0.3) is in good agreement with theoretical predictions in the case of Volmer-Weber growth [16]. The NPs aspect ratio increases from 0.63 (truncated sphere) in the early stage to almost 1 at the end [Fig. 2(b)]. The shape goes to a more stable morphology (isotropic) similar to that obtained without support effect. In order to validate the GISAXS simulations, we performed *ex situ* TEM observations [Fig. 2(c)]. Statistical measurements gave an average diameter of 3.2 nm and an aspect ratio of 0.95. These measurements reported in Figs. 2(a) and 2(b) are in a remarkable agreement with the GISAXS results. The NPs density d is derived from the mean interparticle distance, by assuming one particle per Λ^2 surface. For small amounts of CoPt deposits, we observe a decrease of the NPs density [Fig. 2(b)] that we interpret as a dynamical coalescence, because their diffusion length is larger than their average separation Λ. Since the cluster mobility decreases as a power law when their size increases [17], it is understandable that dynamic coalescence stops after 4 h and the density remains almost constant until the end of the deposition.

GIXD patterns were obtained simultaneously with GISAXS measurements (Fig. 3). The background contribution ($t = 0$ h) is mainly the scattering of the amorphous substrate. Beyond 1 h deposition time, which corresponds to 0.52×10^{15} atoms/cm^2, the metal contribution to the scattered signal can be clearly distinguished from the background and increases with time. For the lowest deposited quantities, background subtraction is a crucial aspect of the data analysis. At these very low deposition times (insert in Fig. 3), the position of the main peak (29–30 nm^{-1}) is shifted, whereas beyond 4 h deposition time, a shoulder develops at 33 nm^{-1} simultaneously with the occurrence of another contribution around 47 nm^{-1}. In the early deposition steps, i.e., during the dynamical coalescence stage, we never observe the fcc structure but rather a noncrystalline atomic arrangement instead (amorphous or multitwinned). For longer deposition times, when the NPs density is nearly constant, the diffraction patterns exhibit the characteristic fcc peaks with an interatomic

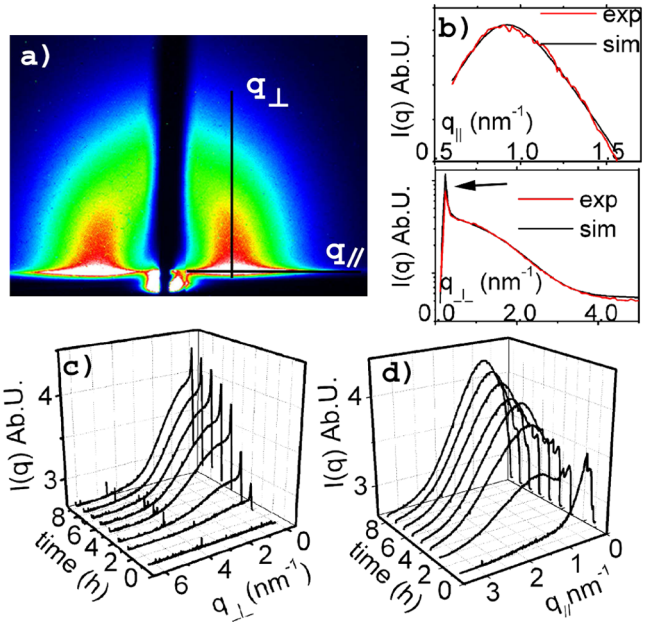

FIG. 1 (color online). (a) Measured GISAXS pattern of sample grown at 500 °C, after five hours corresponding to 2.6×10^{15} atoms/cm^2. The scattering vector q is separated in reciprocal space coordinates $q_\perp$ and $q_\parallel$, perpendicular and parallel to the sample surface, respectively. (b) corresponding cross sections and fits. The arrow shows the Yoneda peak. (c) and (d) graphs show the evolution of $q_\perp$ and $q_\parallel$, respectively, with deposition time.

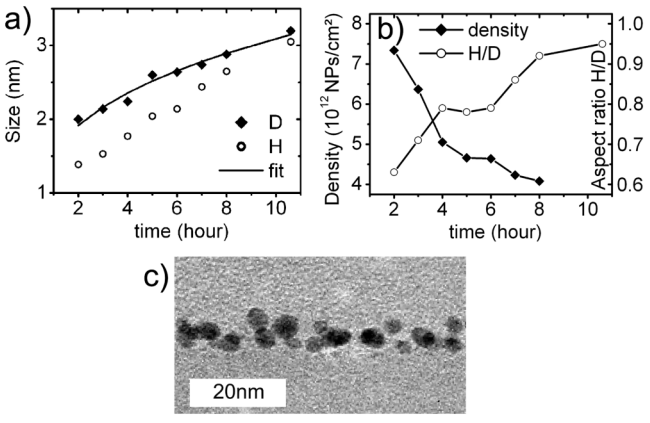

FIG. 2. From the fit of cross sections we deduce the evolution of (a) the mean diameter D and height H ($\pm$ 5%) and (b) the density d of CoPt NPs on the surface (the values at 10.6 h was deduced from TEM measurements) together with the aspect ratio H/D. (c) shows *ex situ* cross section TEM image of the sample.

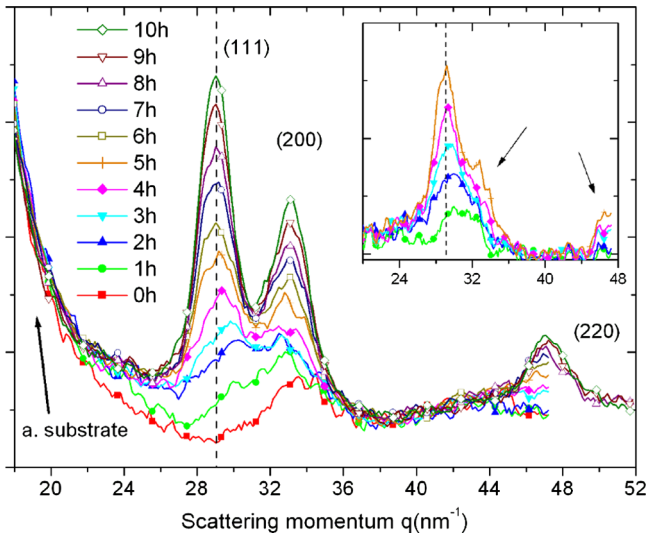

FIG. 3 (color online). Evolution of the GIXD patterns as a function of deposition time. 0 h diffraction data correspond to the background. The inset displays the first scans (up to 5 h) after background subtraction, arrows show fcc additional peaks.

distance of 0.265 nm, close to the fcc disordered bulk value [18], clearly pointing to Co and Pt alloying. However, one may wonder if the structure evolution from a noncrystalline arrangement at the beginning of deposition to a cubic structure after 4 h deposition is linked to the growth mode.

Further interpretation of these measurements requires better knowledge of size and structural effects on the diffraction pattern. The wide-angle scattering intensity for a model cluster i is calculated quantitatively on the basis of the Debye equation [19]:

$$I_{i,N}(q) = \sum_{j} \sum_{j' \neq j} \exp(-\sigma^2 q^2) f_j f_{j'} \frac{\sin(q r_{jj'})}{q r_{jj'}} + S_{\mathrm{inc}}(q),$$

where f_j is the atomic scattering factor of the jth atom. $r_{jj'}$ is the distance between atom j and atom j', and σ^2 is the mean-square displacement in the Debye-Waller prefactor, which expresses the attenuation of the interference term in the Debye equation, due to thermal vibrations or/and static random defects. $S_{\mathrm{inc}}(q)$ is the incoherent scattering function. Preliminary, calculations of the polarization and absorption evolution effects were made but were neglected due to their weak change with q. We have used three structure types in our cluster models: truncated octahedral (TOh) based on face-centered-cubic structure, decahedral (Dh) and icosahedral (Ih) according with Wulff, Marks, and Ino constructions [20], respectively. To fit the diffraction patterns, we used either single size and single cluster type, or a weighted sum of the intensities from several sizes or structures [7]. Models composed of clusters (between 50 and 2000 atoms) with complete shells have been found to be sufficient for data analysis. Monte Carlo simulations of a representative small number of relaxed CoPt cluster structures (TOh, Dh, and Ih illustrated in the inset of Fig. 4) were performed using a semiempirical tight-binding potential [6], to validate the diffraction profiles of these geometrical models [7]. It is worth noting that the possible ordering of the clusters in their low temperature phase has been taken into account in the analysis. However, as mentioned above, in the *in situ* experiments performed at 500 °C, chemical disorder is more probable for NPs smaller than 3 nm as predicted by the Monte Carlo simulations [6].

Figures 4(a) and 4(c) show two stages (5 and 10 h deposition times) of the growth at 500 °C with diameters centered at $D = 2.5$ and 3.2 nm, respectively. For the largest dimension, i.e., cluster with about 1300 atoms, the sample is dominated by fcc clusters, with a small fraction of icosahedral ones (less than 10%). For the smallest dimension, the best fit is obtained with a mix of Ih and TOh-fcc models (around 50% each in atomic fraction) with about 309 and 405 atoms, respectively. Decahedral models were also considered, but no improvement in the fit quality was found. These results show a structural evolution with the NPs size that is predicted in first approximation by energetic stability calculations in metallic clusters [21]. The icosahedral shape is the most energetically stable structure for small dimensions, while fcc clusters are favored for larger ones. Thus, one possible interpretation is that this continuous shape transition, from Ih to TOh structure, is only due to a size effect and the clusters reaching their equilibrium shape during the growth [6].

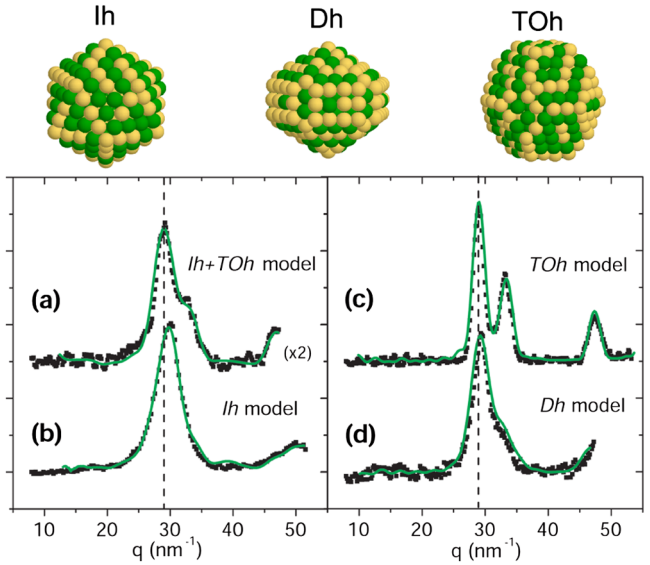

FIG. 4 (color online). Snapshots of icosahedral (Ih), decahedral (Dh) and truncated octahedral (TOh) clusters, and experimental (square marks) and calculated (green or gray solid line) diffraction patterns of similar size distribution samples: $D = 2.5$ nm (a) growth at 500 °C (2.6×10^{15} at/cm^2) and (b) growth at RT (5.2×10^{15} at/cm^2); $D = 3.2$ nm (c) growth at 500 °C and (d) annealing the sample (b) at 500 °C during 1 h. Profiles were offset vertically, and a magnification was applied in one case (in parentheses). A vertical dashed line corresponding to the fcc (111) line of 500 °C grown sample is given for comparison.

However, for small sizes, the 50:50 Ih and TOh-fcc mixture indicates that the sample is still under nonequilibrium conditions. Indeed, the GISAXS results concerning the evolution of the shape and cluster density suggest a coalescence process during the early growth stage. Such events can provide sufficient internal morphological disruption [22] to allow the NPs transformation to the minimum energy morphology, i.e., the TOh shapes at larger sizes [23].

These results have been compared with those obtained for a sample grown at room temperature and then annealed at 500 °C, whose spectra have been chosen to correspond to equivalent cluster sizes:

(i) At room temperature (RT), assuming a size distribution with Gaussian shape (centered between $N = 309$ and 561 atoms), the icosahedral model alone fits the data quite well [Fig. 4(b)]. The growth mechanism at RT is completely different from that at 500 °C: the NPs density is higher (11×10^{12} NP s/cm^2) and the dynamical coalescence is inhibited. After the nucleation stage, the growth at RT corresponds to an atom-by-atom impingement and the initial Ih structure is preserved without transition towards TOh structures [23]. In addition, a shift in the diffraction profile is observed, corresponding to a contraction of the average interatomic distance ($r_i = 0.263$ nm) with respect to the fcc model ($r_i = 0.268$ nm) in the 500 °C sample. Indeed, the contraction is too large to be explained by a thermal effect [6], but is coherent with the denser packing of the Ih structure. For similar NPs size and deposition temperature (RT), Favre *et al.* [4,12] found TOh NPs rather than Ih ones, which could be explained by a matrix effect. Indeed, their NPs were subsequently covered by a thin amorphous silicon layer or embedded in a matrix, thus favoring fcc structures.

(ii) After annealing this sample at 500 °C for 1 h, an average NPs size of 3.2 nm is reached. GIXD refinements [Fig. 4(d)] are consistent with decahedral clusters (centered at $N = 967$) with an average interatomic distance of 0.265 nm. The diffraction signature of Ih and TOh models does not show any similarity with the experimental data. GISAXS measurements indicate that the annealing process induces a decrease of the particle density (6×10^{12} clusters/cm^2) simultaneously with the increase of the particle size from 2.5 to 3.2 nm, which are characteristic of the Ostwald-ripening or static coalescence process [11]. The present structure differs from that of the 500 °C grown sample [Fig. 4(c)] because the kinetic and dynamic history of the samples are different. In the first case (500 °C growth), dynamical coalescence occurs at the early stage of the growth. After this stage, the fcc resulting morphology is locked in and the size increase is dominated by an atom-by-atom growth mechanism. In the second case, the coalescence occurs upon annealing, when the particle size is larger and simultaneously the interparticle distance smaller. Thus, the Dh structure is the result of a quasistatic coalescence [23,24] of Ih structures.

In summary, we have shown, experimentally and with the support of Monte Carlo simulations, the effect of temperature on the structure and morphology of CoPt nanoparticles. Dynamical coalescence in the early stage ($N < 300$ atoms) of growth at 500 °C yields the formation of fcc clusters, while atom-by-atom growth at room temperature produces almost exclusively the nonequilibrium icosahedral morphology. On the other hand, the coalescence from Ih particles (>300 atoms) induced by annealing, yields the formation of decahedral rather than fcc morphology. These *in situ* and real time results bring new understanding of the coalescence versus size effect on small (<3 nm) bimetallic nanoparticle structural transitions at different temperatures.

We acknowledge beam time by the French-CRG of ESRF as well as the help of the BM32 beam line staff. Special thanks to G. Renaud (BM32) for GISAXS training and to T. Sauvage (CERI-Orleans) for RBS facilities.

*Corresponding author.
Pascal.Andreazza@univ-orleans.fr

[1] S. Sun *et al.*, Science **287**, 1989 (2000).
[2] S. Rohart *et al.*, Phys. Rev. B **74**, 104408 (2006).
[3] P. Imperia *et al.*, Phys. Status Solidi (a) (to be published).
[4] P. Moskovkin *et al.*, Eur. Phys. J. D **43**, 27 (2007).
[5] N. Jaouen *et al.*, Phys. Rev. B **76**, 104421 (2007).
[6] G. Rossi, R. Ferrando, and C. Mottet, Faraday Discuss. **138**, 193 (2008).
[7] D. Reinhard *et al.*, Phys. Rev. B **55**, 7868 (1997).
[8] F. Baletto, C. Mottet, and R. Ferrando, Phys. Rev. Lett. **90**, 135504 (2003).
[9] K. Koga, T. Ikeshoji, K. I. Sugawara, Phys. Rev. Lett. **92**, 115507 (2004).
[10] D. Alloyeau *et al.*, Nanotechnology **18**, 375301 (2007).
[11] J. Penuelas *et al.*, Surf. Sci. **602**, 545 (2008).
[12] L. Favre *et al.*, Phys. Rev. B **74**, 014439 (2006).
[13] G. Renaud *et al.*, Science **300**, 1416 (2003).
[14] R. Lazzari, J. Appl. Crystallogr. **35**, 406 (2002).
[15] Y. Yoneda, Phys. Rev. **131**, 2010 (1963).
[16] M. Zinke-Allmang, L. C. Feldman, and M. H. Grabow, Surf. Sci. Rep. **16**, 377 (1992).
[17] P. Jensen, Rev. Mod. Phys. **71**, 1695 (1999).
[18] J. M. Bugnard, Y. Gauthier, and R. Baudoing-Savois, Surf. Sci. **344**, 42 (1995).
[19] B. E. Warren, *X-Ray Diffraction* (Dover, New York, 1990).
[20] L. D. Marks, Rep. Prog. Phys. **57**, 603 (1994).
[21] F. Baletto and R. Ferrando, Rev. Mod. Phys. **77**, 371 (2005).
[22] S. Hendy, S. A. Brown, and M. Hyslop, Phys. Rev. B **68**, 241403(R) (2003).
[23] G. Grochola *et al.*, J. Chem. Phys. **126**, 164707 (2007).
[24] S. Tsyganov *et al.*, Phys. Rev. B **75**, 045421 (2007).